Chemical Engineering Journal 386 (2020) 123791

Contents lists available at ScienceDirect

Chemical Engineering Journal

journal homepage: www.elsevier.com/locate/cej

Restraint of enzymolysis and photolysis of organic phosphorus and pyrophosphate using synthetic zeolite with humic acid and lanthanum

Guoqiang Zhao[a,b], Yanqing Sheng[a,*], Changyu Li[a,b], Qunqun Liu[a,b], Nana Hu[a,b]

[a] Research Center for Coastal Environment Engineering Technology of Shandong Province, Yantai Institute of Coastal Zone Research, Chinese Academy of Sciences, Yantai, China

[b] University of Chinese Academy of Sciences, Beijing, China

HIGHLIGHTS

- Synthetic zeolite loaded with humic acid and La is highly effective for P immobilization.
- La^{3+} and humic acid protect organic P (OP) and pyrophosphate (PP) from photolysis.
- The $La(OH)_3$ can reduce the activity of phosphatase instead of La^{3+}.
- OP and PP complexing with humic acid and/or La^{3+} are resistant to enzymolysis.

GRAPHICAL ABSTRACT

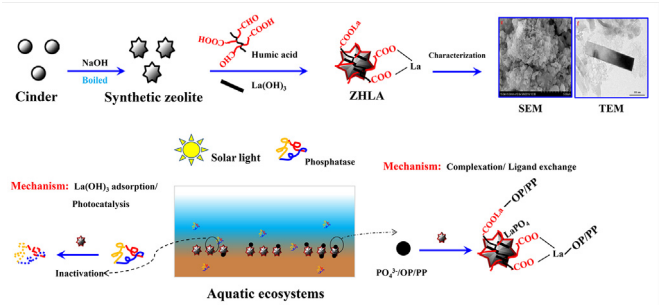

ARTICLE INFO

Keywords:
Organic phosphorus
Pyrophosphate
Immobilization
Synthetic zeolite
Lanthanum
Humic acid

ABSTRACT

Although phosphorus (P)-removing materials have been widely used to immobilize orthophosphate in aquatic ecosystems, the immobilization of organic phosphorus (OP) and pyrophosphate (PP) remains unclear. In this study, a unique OP/PP-immobilizing synthetic zeolite loaded with humic acid (HA) and $La(OH)_3$ nanorod composite (ZHLA) is synthesized, and OP/PP-immobilization is examined by means of enzymolysis and photolysis. The results indicate that OP and PP could not be photodegraded into PO_4^{3-} under natural conditions. Although OP could be degraded into PO_4^{3-} by enhanced Fenton's reagent, La^{3+} and HA could protect OP and PP from degradation. As a result of the colloidal coagulation and photocatalysis of $La(OH)_3$, the activity of phosphatase could be reduced. The PP and phytate become resistant to enzymolysis through the formation of stable HA–La–PP/phytate or La–PP/phytate chelates. However, labile monoester phosphate could not form stable chelates resisting to enzymolysis. This labile monoester phosphate is hydrolyzed into PO_4^{3-} and thereafter immobilized by ZHLA, which is the main pathway to achieve permanent immobilization. Most release-sensitive P fractions are transferred to the stable P fraction after ZHLA application. The ZHLA is demonstrated to be an economical and effective P-immobilization material and has high potential as a commercial sediment-capping product for eutrophication control.

1. Introduction

Phosphorus (P) has been recognized as a limiting factor for algal blooms in aquatic ecosystems [1]. Excessive P can trigger severe eutrophication, leading to harmful algal blooms and deterioration of water quality [2]. In North America and Europe, phosphorus reduction

* Corresponding author.
E-mail addresses: gqzhao@yic.ac.cn (G. Zhao), yqsheng@yic.ac.cn (Y. Sheng), cyli@yic.ac.cn (C. Li), qunqliu@yic.ac.cn (Q. Liu).

https://doi.org/10.1016/j.cej.2019.123791
Received 14 August 2019; Received in revised form 15 November 2019; Accepted 10 December 2019
Available online 12 December 2019

has been widely adopted as a solution to reduce eutrophication [3]. The internal release from sediments and external inputs are two primary sources of P in aquatic ecosystems. Although external loads of P have been increasingly controlled, eutrophication has not been significantly managed because of the release of P from sediments [4]. The immobilization of endogenous P at sediment–water interfaces is therefore essential for eutrophication prevention.

For systematically analyzing the internal P speciation loading, the use of *in-situ* sediment capping agents to immobilize P is one of the most investigated and practical restoration tools [5,6]. The adsorbents containing Fe, Al, and Ca salts have been intensively studied in PO_4^{3-} immobilization [4,7,8]. In this regard, however, Fe is sensitive to changing redox conditions, high pH may reduce the efficiency of Al and Ca because the immobilized P can be substituted by hydroxyl ions, and low pH may enhance the release of toxic Al^{3+} [5]. Currently, the use of rare earth metal-modified adsorbents, including La-modified zeolite and Al $(OH)_3$, is considered as an effective measure to lock PO_4^{3-} from the water column and prevent the release of PO_4^{3-} from the sediment [5,9,10]. The adsorption of PO_4^{3-} is stronger, and the solubility of formed La–PO_4^{3-} complexes is lower than those in Fe, Al, and Ca salts even in a wider pH range [11,12]. This is because the solubility product (Ksp) of La–PO_4^{3-} complexes is particularly low in aqueous and seawater solutions (24.76 and 27.92, respectively), making it the least soluble among rare earth–PO_4^{3-} complexes [6]. The use of these modified P-locked compounds mainly focuses on PO_4^{3-} removal, whereas organic P (OP), pyrophosphate, and/or polyphosphate (PP) have been given less attention.

Organic phosphorous usually shares 12%–42.0% of the total P in sediments [13]. Polyphosphate also constitutes a substantial pool of internal P, especially in eutrophic water with excess P [2,14]. Not only can OP and PP be hydrolyzed into PO_4^{3-} by various phosphatases [15], but they can also be degraded by ·OH in natural water under sunlight [16]. The progress in reducing PO_4^{3-} loads is invalid, however, because the sustained degradation of internal OP and/or PP continues to perform a key function in maintaining eutrophic status [2,17,18]. The comprehensive identification and control of potentially sedimentary bioavailable P (besides PO_4^{3-}) are therefore essential in eutrophication prevention. In recent decades, cost-efficient and environment-friendly P-locking materials have been in urgent demand in geo-engineering for eutrophication control. Coal cinder is the ash of a special coal combustion; this special coal is made of natural powder coal ore (~50%) mixed with red clay and water; it is dried in natural air prior to use. The cinder has a porous and loose structure that makes it more conducive to the adsorption of pollutants. Humic acid (HA) is a widely distributed natural organic matter consisting of various organic compounds formed from decayed biomass [19]. It has a strong metal binding affinity because of its rich aromatic carboxylic acids and hydroxyl functional groups [20]. Humic acid is therefore widely used to remedy heavy metal-polluted sediments and/or soils as well as enhance their buffer capacity and permeability [21]. Most naturally occurring OP and PP present in either monoester or diester form leave one or two non-ester hydroxyl groups to bind HA (HA–OP) or bridge metals (HA–metal–OP) to form stable complexes, which are resistant to hydrolysis by phosphatase [22]. It remains not fully understood whether and how the HA and La composite, which is loaded on the synthetic zeolite, immobilize OP and PP during PO_4^{3-} locking.

The objectives of this study are as follows: (1) to synthesize zeolite/HA/lanthanum (ZHLA) and characterize its properties; (2) to study the mechanisms of ZHLA that restrain OP and PP enzymolysis and photolysis; (3) to investigate the influences of solar irradiation and La speciation on the phosphatase activity; (4) to evaluate the performance of ZHLA-immobilizing PO_4^{3-}, OP, and PP in aquatic ecosystems.

2. Materials and methods

2.1. Sampling and chemicals

Samples are collected from a shallow urban lake in North China (121°25.1′ E, 37°27.7′ N). The lake has a 21-ha surface area with a depth of 1.5–3 m. The overlying water and surface sediments (top 5 cm) at each site are collected and immediately transported to the laboratory for analysis. The pH and dissolved oxygen in the water column are determined *in situ* using a portable multi-parameter probe (YSI Professional Plus, USA). The metal ions of water samples are analyzed using inductively coupled plasma-optical emission spectroscopy (ICP-OES) (Perkin-Elmer Optima 7000 DV, USA). The concentrations of NO_3^-–N, total P (TP), and dissolved PO_4^{3-} in water samples are measured with a continuous flow analyzer (AutoAnalyzer III, Germany). The P fractions and compounds in sediments are analyzed using Ivanoff OP sequential extraction and solution ^{31}P nuclear magnetic resonance (^{31}P NMR) according to the Standards, Measurements and Testing (SMT) protocol. Details of the determination procedures are provided in the Supporting information. The water and sediment properties in the lake are summarized in Table S1.

The HA (Sigma, 53680), purchased from Sigma-Aldrich, is decontaminated according to a previously reported purification procedure [23]. The composition and properties of the purified HA are determined according to the procedure in Ref. [22]. Alkaline phosphatase (AP) (Sigma, P7640) and crude phytase (Sigma, P1259) are also acquired from Sigma-Aldrich. Crude phytase is purified to remove PO_4^{3-} before it is used according to a previous method [17]. Four model OP and/or PP compounds representing a variety of molecular sizes and functional types that are widely found in aquatic ecosystems are obtained from Sigma. These are labile monoester phosphate (adenosine 5′ monophosphate, abbreviated as AMP, Sigma 01930; β-glycerophosphate, abbreviated as β-P, Sigma G9422), condensed-P compounds (abbreviated as PP, Sigma 221368), and phytate (inositol hexakisphosphate, abbreviated as IHP6, Sigma 68388).

2.2. Material synthesis

The coal cinder used in this study is obtained from a local civil heating stove. For the synthesis of zeolite, approximately 50 g of coal cinder filtered through an 80-mesh sieve is placed in a distillation flask and mixed with a 300-mL 2.5-M NaOH solution. The mixture is boiled at 100 °C under reflux conditions for 24 h to generate synthetic zeolite and waste alkaline solution. After the temperature drops to 25 °C, the synthetic zeolite is recovered by centrifugation and washed with Milli-Q water three times, dried at 60 °C, and ground to an 80-mesh size.

The synthetic zeolite/HA is synthesized according to the following procedure: 20 g of synthetic zeolite is added into a 100-mL 0.1% HA-containing waste alkaline solution. The pH of the mixture is thereafter adjusted to 7 using a 0.1-M HCl. Thereafter, the slurry is subjected to ultrasonication for 15 min and shaken for 16 h at 200 rpm.

Using 0.1 M of $LaCl_3{\cdot}7H_2O$ and 10 M of NaOH, $La(OH)_3$ nanorod (a black prismatic crystalline) is synthesized. While stirring, 10 M of NaOH is added dropwise to 0.1 M of $LaCl_3{\cdot}7H_2O$ at 25 °C until the pH level becomes 8.5. It is thereafter subjected to ultrasonification for 15 min. Twenty grams of synthetic zeolite/HA is mixed with 100 mL of $La(OH)_3$ nanorods, subjected to ultrasonication for 15 min, and shaken for 16 h at 200 rpm to synthesize the ZHLA. The aforementioned synthetic zeolite/HA, $La(OH)_3$ nanorods, and ZHLA are recovered and dried using the same procedure as that employed in the synthetic zeolite.

2.3. Characterization of materials

The chemical composition of coal cinder, synthetic zeolite, and ZHLA are determined by X-ray fluorescence analysis (PW2404, Philips,

the Netherlands). The Brunauer–Emmett–Teller specific surface area, total pore volume, and average pore diameter are measured using the nitrogen adsorption method (ASAP 2460, Micromeritics, USA). The morphologies and sizes are imaged by scanning electron microscopy (S-4800, Hitachi, Japan) and transmission electron microscopy (Tecnai G2F20, FEI, USA). The mineralogical composition is identified by powder X-ray diffraction analysis (XRD-7000, Shimadzu, Japan) with Cu-K radiation (40 kV, 30 mA) in the 2θ range of 5°–90°. Fourier transform infrared (FTIR) spectra are obtained using an FTIR spectrometer (Nicolet iS10, Thermo Fisher, USA) with a capacity in the range 4000–400 cm^{-1}. The total acid functional groups and carboxylic acid groups present on the surface of HA are determined by titration (barium hydroxide) and indirect titration (calcium acetate) methods, respectively [23]. The quantity of phenolic hydroxyl groups in HA is the difference between the total quantity of acid functional groups and carboxylic acid groups. The zeta (ζ) potential and particle size of La $(OH)_3$ nanorods, AP, and/or phytase solutions are measured using a potential and particle-sizing analyzer (Zetasizer Nano ZS90, Malvern, U.K.).

2.4. Photolysis and enzymolysis of model OP and PP compounds

Four representative model OP and PP compounds are selected to be used in photochemical and enzymatic degradation experiments. Solutions of model P compounds containing a weighed amount of 2-mM P are prepared, and accurate concentrations are determined after digestion by $H_2SO_4/K_2S_2O_8$ [24]. Next, 30-mM $La(OH)_3$ (pH 8.5) and 0.05% HA (pH 8.5) solutions are prepared. Fenton's reagent is prepared with 600-μM H_2O_2 and 200-μM $FeSO_4{\cdot}7H_2O$ at pH 3. The AP and phytase solutions are prepared in a 0.1-M tris-HCl buffer (pH 9.0) and a 0.1-M NaAc–HAc buffer (pH 5.2), respectively.

First, 5 mL of AMP, β-P, PP, and IHP6 are placed into four tubes, and 5 mL of $La(OH)_3$ and/or HA are thereafter added. The mixture is diluted to 50 mL with Milli-Q water. The pH values of the mixtures are adjusted to 7.0 and thereafter shaken at 200 rpm for 24 h (this reaction time is sufficient to achieve equilibrium as confirmed by the preliminary experiment in Fig. S1).

2.4.1. Photochemical degradation of model P compounds

After 24 h, 2 mL of the abovementioned 50-mL reaction solution is removed and examined according to the photochemical degradation in quartz tubes described below. Thereafter, 8 mL of lake water is screened through a 0.2-μm filter membrane, and/or Fenton's reagent is added. The photolysis experiments are performed in a rotating photoreactor, which is a widely used instrument in photochemical experiments [25]. A 500-W xenon lamp is placed in the center of a cold hydropump, which circulates cooling water. The photoreactor temperature is 28–30 °C. The quartz tubes are placed into the photochemical reactor. The average light intensity on the surface of quartz tubes is approximately 145 ± 5 mW cm^{-2}, as determined using a light intensity test instrument (Newport Corporation, China). The illumination intensity is the same as the direct light intensity on the lake water surface on a midsummer day [16]. The concentration of dissolved PO_4^{3-} in the reaction tubes is determined by the molybdenum blue method at 1, 3, 5, and 16 h.

The steady-state concentration of hydroxyl radicals (·OH) in the filtered lake water and Fenton's reagent under solar irradiation is determined by employing 0.1 M of coumarin as a selective trap [26]. The coumarin can be reacted with ·OH to generate 7-hydroxycoumarin (7-HOC). The concentration of 7-HOC is directly correlated to the steady-state concentration of ·OH. The content of 7-HOC is measured using a calibration curve on a Shimadzu RF-5301 PC spectrometer.

2.4.2. Enzymatic hydrolysis of model P compounds

After 24 h, another 1 mL of the abovementioned 50-mL reaction solution is collected and subjected to the following enzymatic hydrolysis: 0.5 mL of AP solution (2 units (U) mL^{-1} and/or 20 U mL^{-1}, pH 9.0) is added to 1 mL of reaction solutions containing AMP, β-P, and PP. The mixtures are thereafter diluted to 10 mL using 0.1 M of tris-HCl buffer (pH 9.0). In addition, 0.5 mL of phytase (0.1 and/or 1 U mL^{-1}, pH 5.2) is mixed with 1 mL of reaction solutions containing IHP6. The mixture is diluted to 10 mL using 0.1 M of NaAc–HAc buffer (pH 5.2). The above 10-mL enzyme reaction systems are incubated at 37 °C for 16 h. At the end of the reaction, the concentrations of dissolved PO_4^{3-} and the activity of phosphatase in the tubes are determined after shaking using the molybdenum blue method. The AP and phytase are determined according to the *p*-nitrophenol phosphate [12] and vanadium molybdate yellow colorimetric methods [27], respectively.

To determine the effects of HA and/or La on the quantification of PO_4^{3-}, 2 mM of model PO_4^{3-} solution is prepared with KH_2PO_4. The 5-mL model PO_4^{3-} solution is added into four tubes, and then 5 mL of La $(OH)_3$ and/or HA are added. The mixture is diluted to 50 mL with Milli-Q water. The pH values of mixtures are adjusted to 7.0 and thereafter shaken at 200 rpm for 24 h. The amount of PO_4^{3-} in each tube is then quantified after shaking using the molybdenum blue method. The results are summarized in Table S2.

2.5. Effect of La speciation on AP activity

2.5.1. Mixtures of La^{3+} or $La(OH)_3$ and AP under indoor natural light conditions

Two groups of 10-mL reaction tubes are prepared for examining the impact of La^{3+} and $La(OH)_3$ on AP activity. In each group, 0, 0.5, 1, and 2 mL of 30-mM La^{3+} (pH 7.0) and/or $La(OH)_3$ (pH 9.0) solutions are added. At pH 7.0, La is completely ionic (La^{3+} 100%), whereas it is 100% $La(OH)_3$ at pH 9.0 [28]. Thereafter, 1 mL of parallel 2-U mL^{-1} AP solution (pH 7.0 and/or 9.0) is correspondingly added to each group. These mixtures are diluted to 10 mL with a 0.1-M tris-HCl buffer (pH 7.0 and/or pH 9.0). The two groups of tubes are shaken at 200 rpm for 16 h in the laboratory under indoor natural light conditions. Thereafter, a 1-mL mixture is collected to analyze the activity of AP. The pH level of tris-HCl buffer used is consistent with the pH values of $LaCl_3$ (pH 7.0) and $La(OH)_3$ (pH 9.0) during the AP determination.

2.5.2. Mixtures of $La(OH)_3$ and AP with xenon lamp catalysis

Another two groups of ten 10-mL quartz tubes are designed to further investigate the photochemical degradation of AP with $La(OH)_3$ addition under light and/or dark conditions. In each group of tubes, 1 mL of parallel 2-U mL^{-1} AP solution (pH 9.0) is added. Thereafter, 1 mL of 30-mM $La(OH)_3$ at pH 9.0 is placed into five tubes; however, La $(OH)_3$ is not added to the remaining five tubes as controls. All of the above solutions are diluted to 10 mL with a 0.1-M tris-HCl buffer at a pH of 9.0. Two groups of tubes are placed into the photochemical reaction instrument. One group is exposed to a xenon lamp, whereas another group is wrapped in foil. A 1-mL mixture is subsequently collected to analyze the activity of AP in each group at 15 and 30 min, and 1, 3, and 5 h.

2.6. Model P immobilization by ZHLA

2.6.1. Adsorption isotherms

To determine the adsorption isotherms of KH_2PO_4, AMP, β-P, PP, and IHP6, 0.1 g of ZHLA is placed into 100-mL centrifuge tubes to which a 500-mL solution with 5–500 mg L^{-1} model P compounds is added. The gradient concentrations of model P compounds are prepared in a 0.01-M NaCl background to maintain ionic strength. The solution pH is adjusted to 7.0 ± 0.2 and maintained constant with 0.1 M of HCl and/or NaOH. The mixture is stirred at 200 rpm for 48 h until an adsorption equilibrium is reached (this reaction time is sufficient to achieve equilibrium as confirmed by the preliminary experiment in Fig. S2). At the end of the adsorption isotherm experiments, the P concentration in supernatants with KH_2PO_4 addition is directly

determined without $K_2S_2O_8$ digestion. With the addition of the remaining four model P compounds, the P content in supernatants is determined after the digestion with $K_2S_2O_8$. The P concentration is analyzed using the molybdenum blue colorimetric method. To understand the potential ability of ZHLA for P immobilization, data from the adsorption isotherm are fitted to the Langmuir adsorption model, which is given by the following:

$$\frac{Ce}{qe} = \frac{1}{KQ\max} + \frac{Ce}{Q\max} \quad (1)$$

where Qmax ($mg{\cdot}g^{-1}$) is the maximum adsorption capability, and qe ($mg{\cdot}g^{-1}$) is the equilibrium adsorption capacity; *K* is the binding constant, which is related to adsorption strength ($L{\cdot}mg^{-1}$), and Ce ($mg{\cdot}L^{-1}$) is the equilibrium concentration.

2.6.2. Enzymatic hydrolysis of model P compound ZHLAs

To investigate the stability of fixed OP/PP by ZHLA under enzymolysis and photolysis conditions, 0.4 g of ZHLA is extracted by 1 mM of AMP, β-P, PP, and IHP6 for 48 h and then lyophilized for the subsequent experiments.

Two grams of lyophilized ZHLA onto which model P compounds adsorb is weighed into four quartz tubes. The amount of model P compounds that adsorbs onto the 0.2-g ZHLA in each tube is calculated as "Q_a" (mg of P). Thereafter, 10-mL AP buffer solutions (2 U mL^{-1}, pH 7.0) and/or tris-HCl buffer (pH, 7.0) are added into the four tubes with AMP, β-P, and PP. Meanwhile, 10-mL phytase (0.2 U mL^{-1}, pH 7.0) and tris-HCl buffer (pH 7.0) are added into the tube containing IHP6. All tubes are placed into the photochemical reaction instrument and stirred using magnetic stirrers for 16 h. Then, the mixtures in the tubes are centrifuged, and aliquots of the supernatant are collected for the quantification of PO_4^{3-} and TP with or without $K_2S_2O_8$ digestion. The difference between TP and PO_4^{3-} is OP or PP. The degradation rate of model P compounds in supernatants is calculated from the ratio of PO_4^{3-} in the supernatant to the corresponding Q_a. The desorption rate of model P compounds in the supernatants is calculated from the ratio of OP or PP in the supernatant to the corresponding Q_a.

After centrifugation and washing with saturated NaCl solutions, the residues are lyophilized for the remaining P measurements. The TP in dried residues is determined by calcination in a muffle furnace at 550 °C and thereafter extracted using a 1-M solution of HCl. The PO_4^{3-} in the residues is directly extracted by 1 M of HCl for 16 h without calcination. The difference between TP and PO_4^{3-} is OP or PP [29]. The degradation rate of model P compounds in the residues is calculated from the ratio of PO_4^{3-} in the residues to the corresponding Q_a. The percentage of unhydrolyzed model P compounds in the residues is calculated from the ratio of OP or PP in the residues to the corresponding Q_a. The PP could be evidently hydrolyzed into PO_4^{3-} during the extraction by 1 M of HCl. The hydrolysis rate of 1-mM model P compounds with an extraction of 1 M of HCl for 16 h is detected. The hydrolysis rate of PP by HCl is utilized to determine the true content of PP in the residue. The correction details are summarized in the Supporting information.

2.6.3. Changes of P fractions in sediment after ZHLA addition

Approximately 5 g of sediments is placed into a conical flask, and 200 mL of filtered lake water (0.45 μm) is added. After different doses (0.25%, 0.5%, and 1%) of ZHLA are scattered, the mixed slurries are left to stand at 28–30 °C for a 28-d incubation. After the incubation, P in the supernatant is analyzed. The residues are then lyophilized for the P fraction measurement. The P fractionation procedure is thereafter implemented for both original and ZHLA-dosed sediments according to the SMT and Ivanoff sequential extraction method. The detailed operating steps are summarized in the Supporting information.

2.7. Toxicity analysis of La and Al

Excessive Al^{3+} and La^{3+} may be toxic to sensitive species present in water [30,31]. Batches of La and Al-releasing experiments are therefore conducted. First, 1 $g{\cdot}L^{-1}$ of ZHLA is prepared in a 0.01-M NaCl at pH levels of 5, 7, 8, and 9. The slurries are thereafter shaken for 48 h at 28–30 °C. The concentrations of released Al and La are analyzed by ICP-MS (ELAN DRC II, Perkin-Elmer, USA).

2.8. Statistical analysis

Data significance is analyzed using one-way analysis of variance, followed by mean testing between the control and treated groups and/or among different treated groups using SPSS 20.0. Data and homogeneity of variance are tested using Student–Newman–Keuls multiple range tests and Bartlett's test, respectively. The thermodynamic states of La^{3+} and Al^{3+} at pH values of 2–13 are simulated using Visual MINTEQ 3.0.

3. Results and discussion

3.1. ZHLA characterization

Coal cinder, synthetic zeolite, and ZHLA are mainly composed of approximately 45%, 30%, 6%, and 4.5% of Si, Al, Ca, and Fe, respectively. This indicates that oxides and/or hydroxides of Al, Ca, and Fe are the three important components in the starting material (cinder). These metal compounds are conducive to P adsorption [6]. Compared with cinder and synthetic zeolite, ZHLA has a higher La content (4.9%) because of the formation of $La(OH)_3$ (Table 1). The XRD results are shown in Fig. 1. The XRD analysis further suggests that quartz (SiO_2) and mullite ($Al_6Si_2O_{13}$) compounds in the cinder mainly contain Si and Al. The synthetic zeolite is identified as a type of NaP1 zeolite ($Na_6A1_6Si_{10}O_{32}{\cdot}12H_2O$), which is an ideal zeolite with a considerable ion exchange capacity and a large specific surface area [32,33]. The peaks in the XRD pattern of ZHLA are the same as those exhibited by synthetic zeolite although the intensity of some peaks are reduced because of the greater absorption and stronger diffusion of X-ray radiation by heavy La^{3+} cations [9]. The synthesized $La(OH)_3$ nanorods are identified as $La(OH)_3$ crystal phase (PDF#36-1481) (Fig. S3).

The specific surface areas and total pore volumes of synthetic zeolite (32 $m^2{\cdot}g^{-1}$ and 0.2 $cm^3{\cdot}g^{-1}$) and ZHLA (49 $m^2{\cdot}g^{-1}$ and 0.2 $cm^3{\cdot}g^{-1}$) exhibit an evident increase compared with cinder (8 $m^2{\cdot}g^{-1}$ and 0.02 $cm^3{\cdot}g^{-1}$). This indicates that a porous structure of synthetic zeolite and ZHLA with large specific surface areas is formed. The average pore diameters, however, remain practically constant (~4 nm), demonstrating that alkaline erosion and La and HA addition could not change the mesoporous size of cinder. The SEM images further verify that the

Table 1
The chemical composition (%), specific surface area ($m^2\ g^{-1}$), total pore volume ($cm^3\ g^{-1}$) and average pore diameter (nm) of clinker, synthetic zeolite, and ZHLA on dry base.

Item	Clinker	Zeolite	ZHLA
SiO_2	47.82	44.94	45.16
Al_2O_3	32.73	30.10	31.39
CaO	7.15	5.76	4.91
Fe_2O_3	5.48	3.85	4.35
K_2O	1.90	0.888	0.681
Na_2O	1.39	12.28	5.91
TiO_2	1.06	0.900	0.955
MgO	1.01	0.712	0.783
La_2O_3	N.D.	N.D.	4.90
Other[a]	0.62	0.59	0.61
LOI[b]	9.20	4.50	9.30
Specific surface area	8	32	49
Pore volume	0.02	0.2	0.2
Pore diameter	4	4	4

[a] Including MnO, Cl, AgO, ZrO_2, and etc.
[b] Loss on ignition.

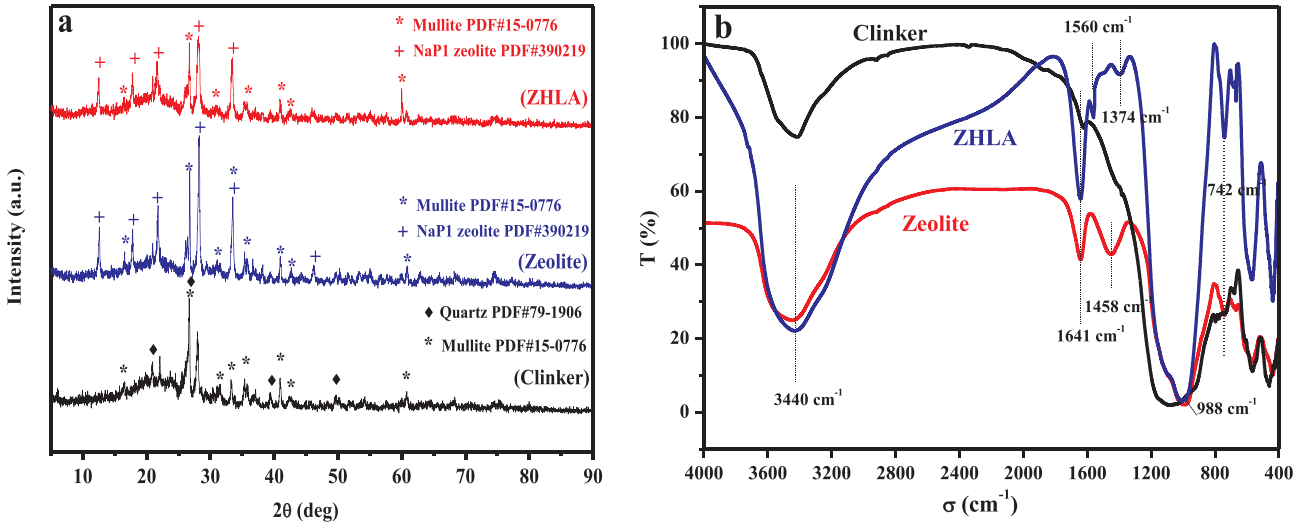

Fig. 1. (a) XRD patterns of clinker, synthetic zeolite and ZHLA. *: mullite; ♦: quartz; +: NaP1 zeolite. (b) FTIR spectra of clinker, zeolite and ZHLA.

cinder surface is a dense block structure, whereas the surface of synthetic zeolite has a typical honeycomb and porous structure (Fig. 2a and c). The SEM images in Fig. S4 also provide information related to the average particle size of cinder, synthetic zeolite, and ZHLA, which are approximately 3–5, 1.5, and 1 μm, respectively. The foregoing indicates that the synthetic process of ZHLA has the tendency to reduce the particle size of cinder to become more conducive to P absorption. The SEM images of ZHLA indicate that $La(OH)_3$ has a rod-like structure (Fig. S5). The TEM images further confirm that the internal structure of cinder is generally homogeneous and compact, whereas the edge of synthetic zeolite is corroded into irregular columns. In contrast, the ZHLA coated by HA and $La(OH)_3$ appear in a fine dispersive state and an embedded black crystal. Previous studies report that $La(OH)_3$ nanorods exhibit a black prismatic crystalline form that is 50–200 nm in diameter [34]. The TEM image clearly demonstrates that HA and $La(OH)_3$ are successfully loaded onto the synthetic zeolite (Fig. 2f).

The FTIR of synthetic zeolite and ZHLA are analyzed. The broad peak of approximately 3400 cm^{-1} is related to the stretching vibration of H–O–H of the cinder/zeolite structure [35]. The peak at 1641 cm^{-1} is attributed to the H–O–H symmetric vibration of lattice water in the cinder/zeolite [36]. The peak intensity of 1641 cm^{-1} in synthetic zeolite and ZHLA is evidently enhanced because the pores and specific surface area are significantly higher than those in the cinder, which is capable of adsorbing more water. The peaks at 988 and 742 cm^{-1} are ascribed to the asymmetric stretching vibration of internal tetrahedral models of O–T–O bonds in TO_4 (where T denotes Si, Al, or Fe) and an external symmetrical stretching vibration of O–T–O bonds, respectively [33,36]. Phenolic hydroxyl groups and carboxylic acid groups are the two primary function groups in terms of the chelating chemistry of HA. Compared to synthetic zeolite, the ZHLA exhibits two new absorption peaks that appear at approximately 1560 and 1370 cm^{-1} after HA is loaded. The peak at 1560 cm^{-1} is the asymmetric vibration peak of COO^-, and the peak at 1370 cm^{-1} is the symmetric vibration peak of COO^- [37]. This indicates that La^{3+} and/or other metal ions (M^{n+}: Al, Fe, and Ca) could be chelated with HA (HA–M^{n+}) by the formation of O═C–O–M^{n+}. The content of acid functional groups in the HA indicates that the phenolic hydroxyl groups and carboxylic acid groups are 2.1 and 3.2 $mmol{\cdot}g^{-1}$, respectively (Table S3). Apart from carboxylic acid groups, phenolic hydroxyl groups are another important functional groups that chelate M^{n+} as "Ar–O–M^{n+}" complexes [19].

3.2. Influence of HA and La on photolysis of model P

Compared to the background value of PO_4^{3-} in filtered lake water, PO_4^{3-} is basically constant with no significant differences ($p > 0.05$) in the tubes with model P compounds under solar irradiation (Table S4). This means that AMP, β-P, PP, and IHP6 could not be degraded into PO_4^{3-} by solar lights under natural conditions with a sufficient steady-state concentration of ·OH ($6.5 \pm 0.10 \times 10^{-16}$ M calculated from Fig. S6). Li et al. [16] reported, however, that OP in natural lakes could be significantly photodegraded into PO_4^{3-} even with an ·OH content of considerably less than 6.5×10^{-16} M. The key reason for the discrepancy is that OP and PP have undergone autoclaved treatments in the experiments of Li et al. Some OP/PP (β-P and PP) are thermally decomposed (Fig. S7), and ~20% AMP and β-P, and ~90% PP could be hydrolyzed into PO_4^{3-} after autoclaving treatments (Fig. S8). Abundant PO_4^{3-} is therefore released from autoclaved sediments under solar irradiation mainly because of the thermal hydrolysis of OP/PP rather than photolysis (Table S5).

To investigate the OP/PP resistance to enhanced photolysis in the presence of $La(OH)_3$ and/or HA, the steady-state content of ·OH is significantly enhanced by the addition of Fenton's reagent. The calculated steady-state concentration of ·OH in Fenton's reagent is ~62 times higher than that in lake water systems. Fig. 3 shows that in Fenton's reagent under solar irradiation, approximately 90% AMP and 100% β-P are degraded into PO_4^{3-} after 5 h. The photolysis proportion of IPH6, however, is only 25% with no photolysis for PP after 16 h. This shows that AMP and β-P are more easily hydrolyzed into PO_4^{3-} by the enhanced photolysis than PP and IPH6. The photolysis amounts of OP and PP, however, significantly decrease in the presence of HA ($p < 0.05$). This could be attributed to HA that hinders the photolysis of target compounds by either absorbing the available light [38] or scavenging the produced free radicals [39]. The photolysis amounts of AMP, β-P, and IHP6 further drop significantly with the presence of La $(OH)_3$ ($p < 0.01$), which could probably generate stable OP–La chelates to avoid enhanced photolysis [22]. Previous studies indicate that metal ions could slightly catalyze the hydrolysis of PP to PO_4^{3-} [40,41]. The slight hydrolysis of PP in the tube with the addition of La from 0 to 16 h is therefore probably caused by the catalysis of La^{3+} rather than the enhanced photolysis. The results demonstrate that HA and/or $La(OH)_3$ could protect OP and PP from hydrolyzing into PO_4^{3-} by enhanced radical oxidation.

3.3. Influence of HA and La on enzymolysis of model P

The results shown in Fig. 4a reveal that the four model P compounds could all be completely hydrolyzed into PO_4^{3-} by AP, indicating that free OP and PP could be easily hydrolyzed into PO_4^{3-} by phosphatase.

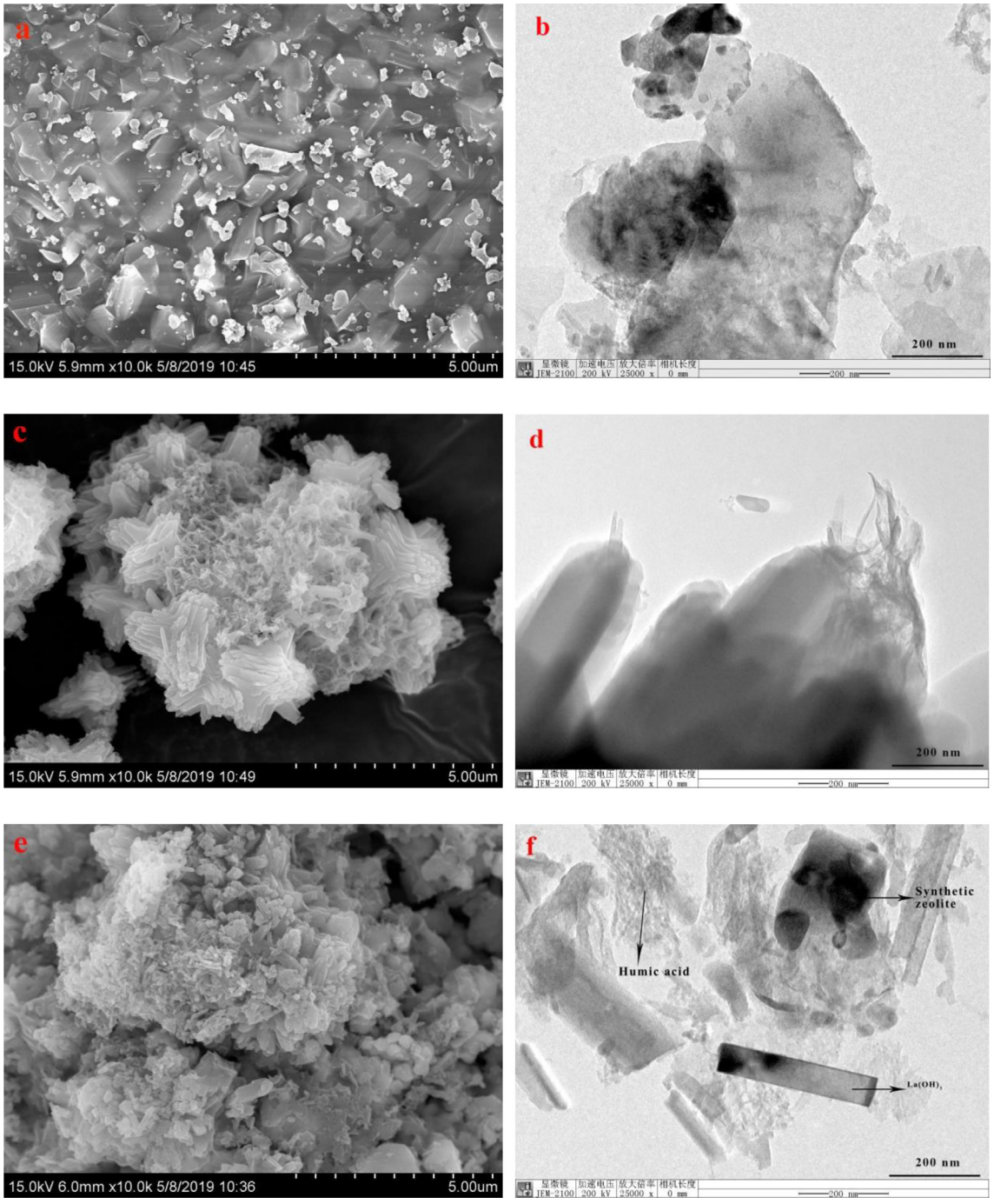

Fig. 2. SEM images of clinker (a), synthetic zeolite (c) and ZHLA (e). TEM images of clinker (b), zeolite (d) and ZHLA (f).

The hydrolysis rate of model P compounds is significantly reduced by the addition of $La(OH)_3$ or $La(OH)_3$ and HA ($p < 0.05$), demonstrating that La and/or HA prevent the enzymatic hydrolysis of OP and PP. Fig. 4b shows that the activity of AP in the tubes with the addition of $La(OH)_3$ or $La(OH)_3$ and HA is significantly lower than that in the tubes with only model P ($p < 0.05$). The activity of phytase, however, basically remains constant in all tubes. This demonstrates that $La(OH)_3$ could probably reduce the AP activity rather than the phytase activity because the entire amount of $La(OH)_3$ has been changed into La^{3+} at pH 5.2 (confirmed in Fig. S9). Fig. 4c illustrates that APM and β-P could be completely hydrolyzed into PO_4^{3-} with the presence of $La(OH)_3$ or $La(OH)_3$ and HA by phosphatase with a higher activity (called enhanced phosphatase). The hydrolysis of PP and IHP6, however, remains approximately constant. The activity of enhanced phosphatase is shown in Fig. 4d. The foregoing result reveals that the decrease in the enzymolysis of AMP and β-P can probably be attributed to the reduction in the AP activity by $La(OH)_3$ instead of the formation of stable OP chelates. The enhanced phosphatase remains incapable of hydrolyzing PP and IHP6, which can be attributed to the generation of stable PP–La and IHP6–La or PP–HA–La and IHP6–HA–La chelates [22]. This is because PP and IHP6 are excellent chelating agents that can make complex metal ions become recalcitrants in natural environments [14,42].

To confirm the formation of stable chelates of PP–La and IHP6–La or PP–HA–La and IHP6–HA–La, the FTIR of spectra of solutions of PP, IHP6, and HA with and/or without the addition of La is determined (Fig. 5). Fig. 5a shows that a peak appeared at 1160 cm^{-1} in the FTIR of

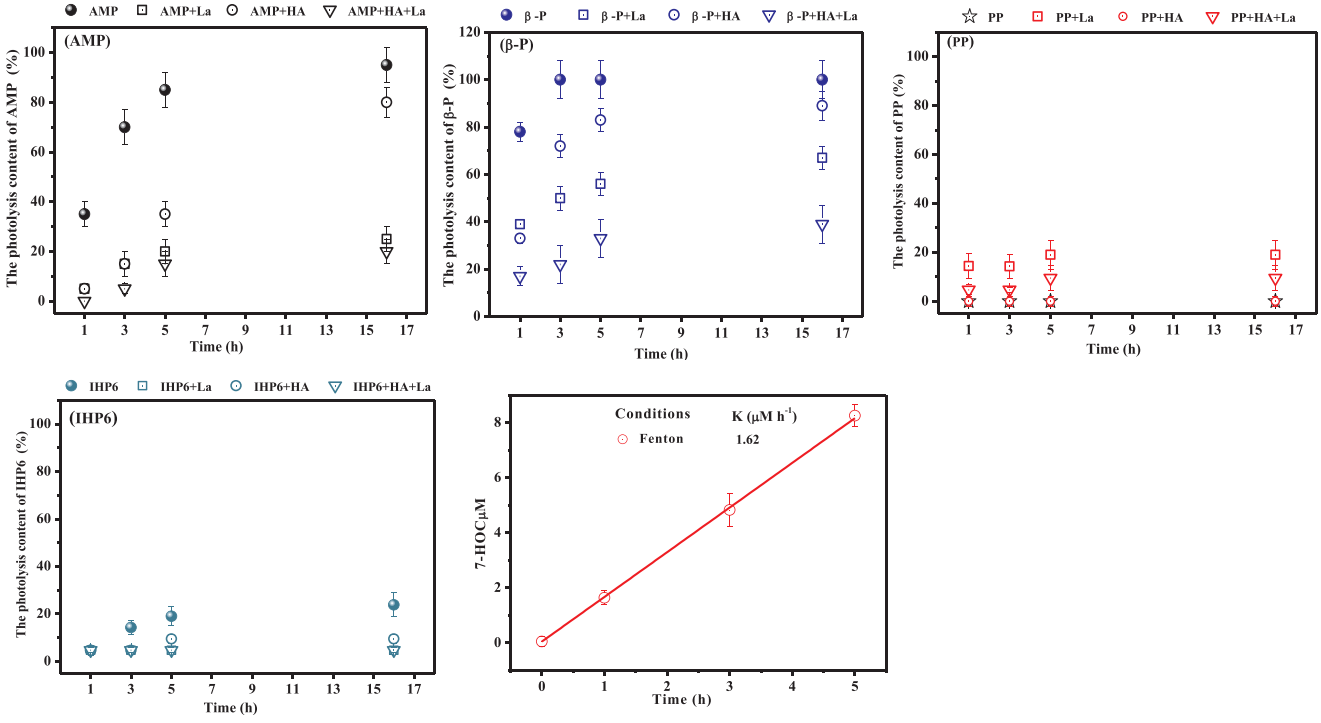

Fig. 3. The photolysis of the model P compounds and the content of 7-HOC were in the Fenton's reagent under solar irradiation.

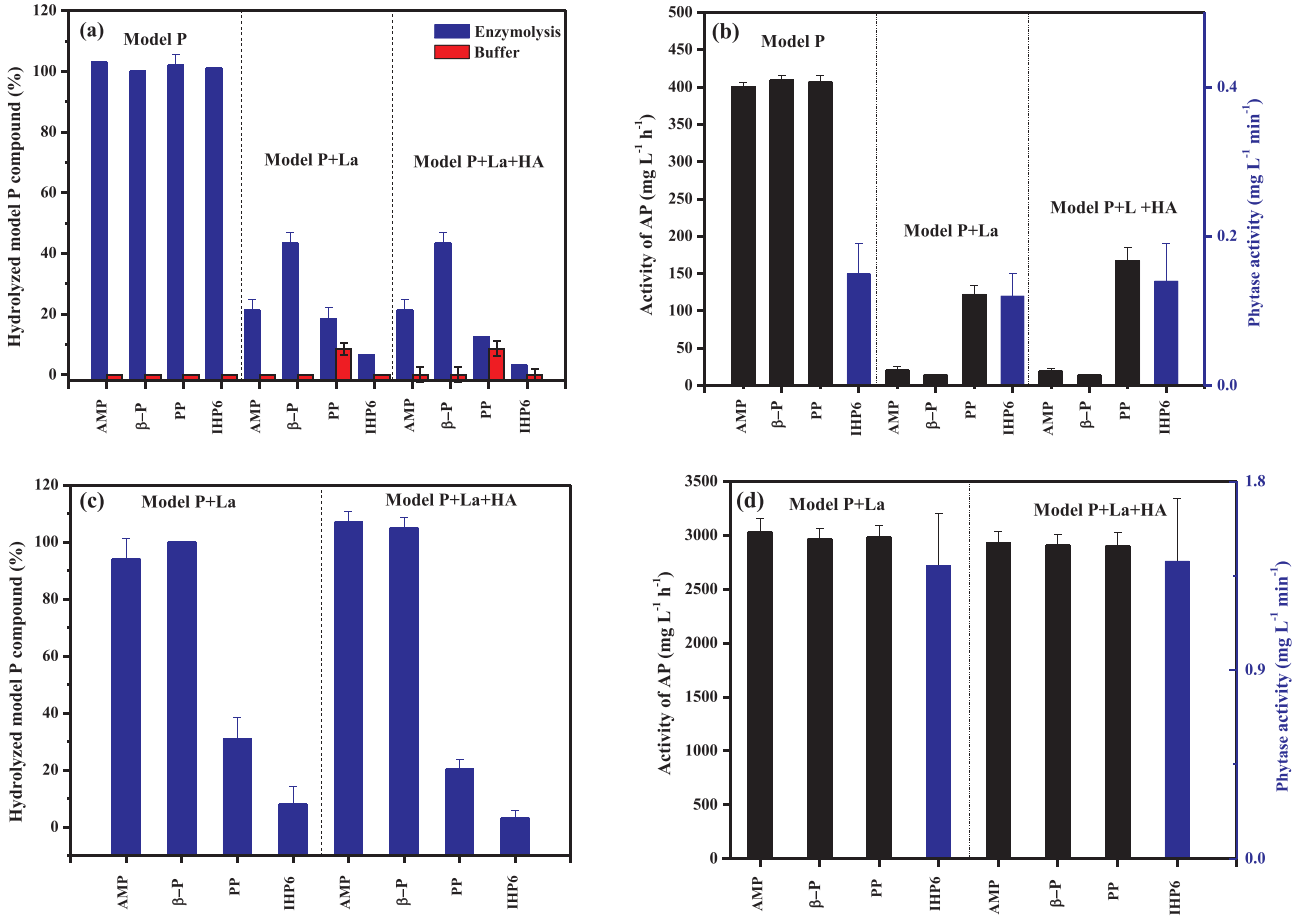

Fig. 4. Effect of HA and La on enzymatic hydrolysis of model P compounds: (a) The hydrolysis under low enzyme activity (AP, 2 U mL^{-1}; phytase, 0.1 U mL^{-1}); (b) The activity of AP and/or phytase in the tubes with lower enzyme activity; (c) The hydrolysis under high enzyme activity (AP, 20 U mL^{-1}; phytase, 1 U mL^{-1}); (d) The activity of AP and/or phytase in the tubes with higher enzyme activity.

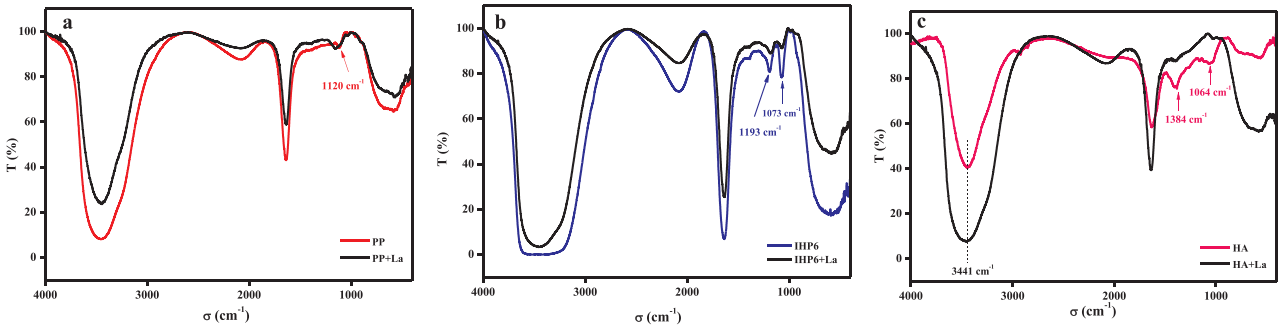

Fig. 5. FTIR spectra of solutions of (a) PP with or without the addition of La; (b) IHP6 with or without La; (c) HA with or without La.

the PP solution. The symmetric and antisymmetric stretching frequencies of P–O$^-$ bond in PP are generally observed in the range 1170–1000 cm^{-1} [43]. This P–O$^-$ peak, however, slightly shifts to a higher wavenumber side with the presence of La^{3+}, indicating that the combination of La^{3+} and P–O$^-$ affects its wavenumber [44]. This confirms the formation of stable chelates of PP–La via P–O$^-$ bond in PP. Fig. 5b shows that in the FTIR of IHP6, two peaks appear. These two peaks, 1193 and 1073 cm^{-1}, are attributed to the vibration of P═O bonds and P-OH bonds in IHP6, respectively [45]. The intensities of the two peaks, however, both decrease with a slight shift to the lower wavenumber side in the presence of La^{3+}, which is demonstrated to affect the two bonds. This confirms that IHP6 should be chelated with La via P═O and P–OH bonds. Fig. 5c shows that two peaks, 1384 and 1064 cm^{-1}, appear in HA, and their intensities decrease when La^{3+} is added. The peak loaded at 1384 cm^{-1} is identified as a C═O symmetric stretching in COO$^-$ groups. The peak of 1064 cm^{-1} is a stretching vibration of C–O and bending vibration of O–H [19]. In addition, the stretching vibration intensity of O–H at 3441 cm^{-1} of HA increases with the presence of La^{3+}, indicating the involvement of O–H groups in metal ion complexation resulting from the formation of aqua complexes [19,46]. This confirms the formation of HA–La chelates mainly through COO$^-$ groups, OH groups, and C–O bond. It is therefore highly possible for one side of La^{3+} to associate with HA and the other side with PP or IHP6 through the related function groups and bonds when HA and P model compounds exist at the same time. This justly confirms the formation of PP–HA–La and IHP6–HA–La chelates.

3.4. Effect of La^{3+} and $La(OH)_3$ on AP activity

As shown in Fig. 6a, the activity of AP significantly decreases as $La(OH)_3$ increases ($p < 0.01$), whereas in the presence of La^{3+} ($p > 0.05$), it remains basically constant, indicating that $La(OH)_3$ is the main species inhibiting AP activity rather than La^{3+}. The results shown in Fig. 6b indicate that the activity of AP remains practically constant without the addition of $La(OH)_3$ as a control in the dark; however, the activity of AP in the control significantly drops with time under solar irradiation. The comparison suggests that solar light could evidently reduce the AP activity. In the experimental groups with the addition of $La(OH)_3$, the activity of AP exhibits a significant downward trend under both dark and light conditions ($p < 0.05$); the decline, however, is more distinct under light conditions. This shows that $La(OH)_3$ itself could inhibit AP activity without solar irradiation, which could enhance the inhibition capability by $La(OH)_3$. Fig. 6c indicates that the zeta potential of $La(OH)_3$ is positive, but the AP and phytase are both negative when the pH ranges 5–9. This indicates that the synthetic $La(OH)_3$ nanorod is a positively charged colloid in the solution; however, the two phosphatases are negatively charged colloids in the solution. Fig. 6d shows the particle size of $La(OH)_3$ solution ranging from 10 to 100 nm, which confirms that it is a colloidal solution. The average particle size of AP solution is approximately 130 nm. The average particle size of the solution with the addition of AP and La $(OH)_3$, however, significantly increases to approximately 1600 nm with the formation of macroscopic coagulations in the tube bottom (Fig. S10). The AP is therefore absorbed and coagulated by the $La(OH)_3$ colloid through electrostatic attraction, resulting in the decrease in the AP activity. In addition, $La(OH)_3$ nanorods have a photocatalytic activity that can produce superoxide radicals ($\cdot O_2$) [47]. Organic matter can be indirectly degraded by generating $\cdot O_2$ under solar irradiation [47,48]. The inhibition of AP activity is therefore enhanced by $La(OH)_3$ under solar irradiation.

3.5. Immobilization of P by ZHLA

Adsorption data are well fitted by the Langmuir model (Table S6). The calculated Q_{max} values for PO_4^{3-}, AMP, β-P, PP, and IHP6 are 26.2, 6.2, 5.38, 15.8, and 17.5 mg·g^{-1}, respectively. The adsorption of PO_4^{3-} by ZHLA is primarily attributed to $La(OH)_3$ in the materials. The La L_{III}-edge extended X-ray absorption fine structure analysis indicates that PO_4^{3-} is bonded to La sites in materials that contain $La(OH)_3$ primarily by forming inner sphere bidentate–binuclear complexes and oxygen defects, which could be active adsorption sites for PO_4^{3-} [10]. Bonding with La^{3+} or HA–La^{3+} in the ZHLA to form La–OP or HA–La–OP/PP chelates is the main adsorption mechanism of OP and PP [22].

Fig. 7a shows that PO_4^{3-} is not detected in the supernatant of each tube between the enzymatic treatment and buffer control. The results indicate that AMP, β-P, PP, and IHP6 immobilized by ZHLA could not release any PO_4^{3-} from ZHLA into the overlying water under enzymolysis. Fig. 7b illustrates that practically no OP and PP is detected in all the supernatants. This suggests that AMP, β-P, PP, and IHP6, which could not be desorbed into the overlying water under enzymolysis conditions and stirring, are firmly immobilized by ZHLA. The results in Fig. 7c demonstrate that PO_4^{3-}–P, which accounts for ~74% and ~68% of the total adsorbed AMP and β-P (Q_a), respectively, in the ZHLA are detected in the residue of the enzymolysis group, whereas PO_4^{3-} is not detected in residues of buffer controls. Although phosphatase could hydrolyze part of the AMP and β-P into PO_4^{3-} in the ZHLA, the hydrolyzed PO_4^{3-} could probably be captured by $La(OH)_3$ in the ZHLA via ligand exchange as a stable $LaPO_4$ compound. This protects PO_4^{3-} from being released into overlying water. In addition, lower PO_4^{3-}–P values that account for ~40% and ~3% of the total adsorbed PP and IHP_6 (Q_a), respectively, in the ZHLA are detected in the residues of the enzyme treatment group; however, the amounts of PO_4^{3-}–P in the residues of their buffer controls remains ~40% and ~1%, respectively. The corrected amount of PO_4^{3-}–P from PP in the residues is ~16% because ~62% of PP could be directly hydrolyzed into PO_4^{3-} by HCl during extraction (Table S7). Approximately 16% of adsorbed PP is still hydrolyzed into PO_4^{3-} in the buffer control; this is mainly attributed to its catalytic hydrolysis by metal ions in ZHLA [40,41]. Small amounts of PP or IHP6 are thus hydrolyzed into PO_4^{3-} by phosphatase in the residues. Fig. 7d further confirms that ~85% of PP and ~97% of IHP6 remain unhydrolyzed in the residue after enzyme treatment, whereas the remaining unhydrolyzed AMP and β-P in the

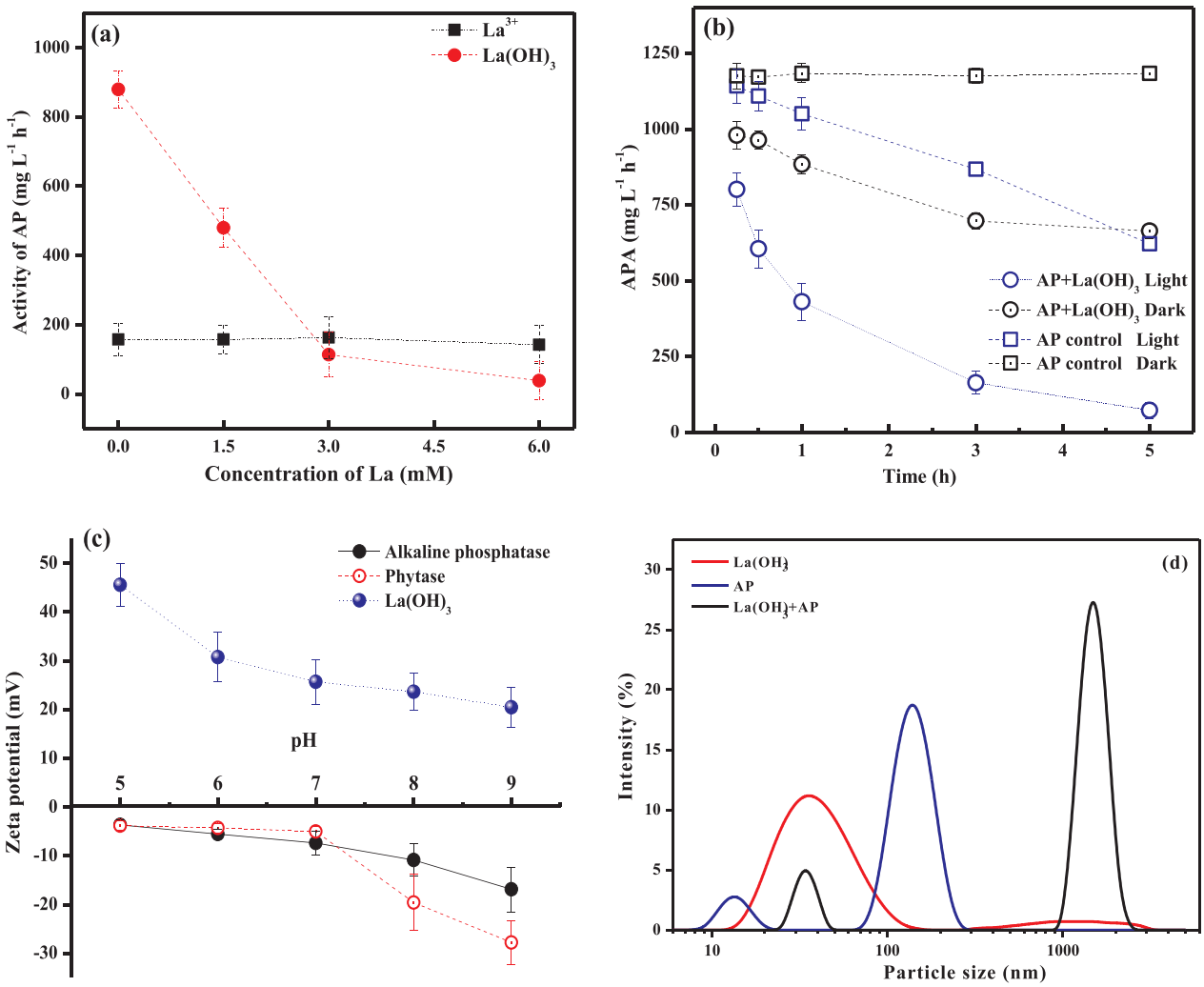

Fig. 6. (a) Effect of La^{3+} and $La(OH)_3$ on the activity of AP. (b) Effect of $La(OH)_3$ on the activity of AP under light and/or dark conditions. (c) Zeta potential of enzymes and $La(OH)_3$ in solutions with different pH. (d) Particle size of $La(OH)_3$ solution, AP solution, and mixed solution of $La(OH)_3$ + AP at pH 9.0.

residue are only ~25% and 30%, respectively. More than 90% of adsorbed AMP, β-P, and IHP6, and 80% of adsorbed PP are still preserved in the residues that are not hydrolyzed into PO_4^{3-} in the buffer control group. The AMP–La and β-P–La, AMP–La–HA, or β-P–La–OP chelates are thus more easily hydrolyzed into PO_4^{3-} than PP and IHP6 by phosphatase. The unhydrolyzed AMP and β-P in residues are probably caused by the reduction of AP activity to lower levels by ZHLA through absorption and $La(OH)_3$ photolysis. The PP–La or IHP6–La and PP–HA–La or IHP6–HA–La chelates are more stable and resistant to enzymolysis.

3.6. Potential engineering implications

The results shown in Fig. 8a indicate that the maximum concentrations of released Al^{3+} and La^{3+} are 0.43 and 12.9 mg·L^{-1} between pH values of 5 and 9 with low eco-toxicity that are significantly lower than 3.9 and 23 mg·L^{-1} [10]. Fig. 8b shows that the reason for the low release of Al^{3+} is that the thermodynamic states of Al mainly exist as solid Al compounds (diaspore) rather than Al ions between pH values of 5 and 9. Compared with the contents of released La^{3+} at a pH of 7–9, a higher content is found at pH 5 primarily because approximately 100% of La exists as La^{3+}. Although all of the La can change into La^{3+} at a pH value below 7, the released La^{3+} (12.9 mg·L^{-1}) at pH 5 remains lower mainly because HA–La chelates protect it from being released [10]. This confirms that the application of ZHLA is ecologically safe without causing substantial adverse effects to the aquatic ecosystem. Fig. 8c shows that the release-sensitive inorganic P (NaOH–Pi) significantly decreases ($p < 0.01$), whereas the stable Pi (HCl-Pi) evidently increases ($p < 0.01$) with increased ZHLA. The Pi of sediments is divided into NaOH-extractable Pi (NaOH-Pi) and HCl-soluble Pi (NaOH-Pi) by the classical SMT protocol. The NaOH–Pi is easily released into overlying water as soluble reactive PO_4^{3-}, whereas HCl–P is extremely stable to be easily regenerated [49]. In addition, labile OP and moderately labile OP significantly decrease ($p < 0.01$), but non-labile OP dramatically increases ($p < 0.01$) after incubation. The OP of sediments is classified as labile OP, moderately labile OP, and non-labile OP using the Ivanoff OP sequential extraction method. Labile OP is the most reactive OP fraction and is easily hydrolyzed into soluble reactive PO_4^{3-}, whereas non-labile OP is the most stable fraction and has a strong resistance to hydrolysis [50]. Excellent performances for the immobilization of both Pi and OP are therefore exhibited by ZHLA.

The raw material for ZHLA production is available at a low cost. The cost to produce one metric ton of ZHLA is estimated to be ~$105. Calculating the Q_{max} of each fraction of P in this ZHLA, one metric ton of ZHLA can immobilize approximately 26 kg of PO_4^{3-}, 5 kg of labile monoester phosphate, 15 kg of PP, and 17 kg of IHP6. Furthermore, the cost of ZHLA is significantly lower than lanthanum/aluminum hydroxide composite ($1200/t) and commercial Phoslock ($240/t) [10]. The

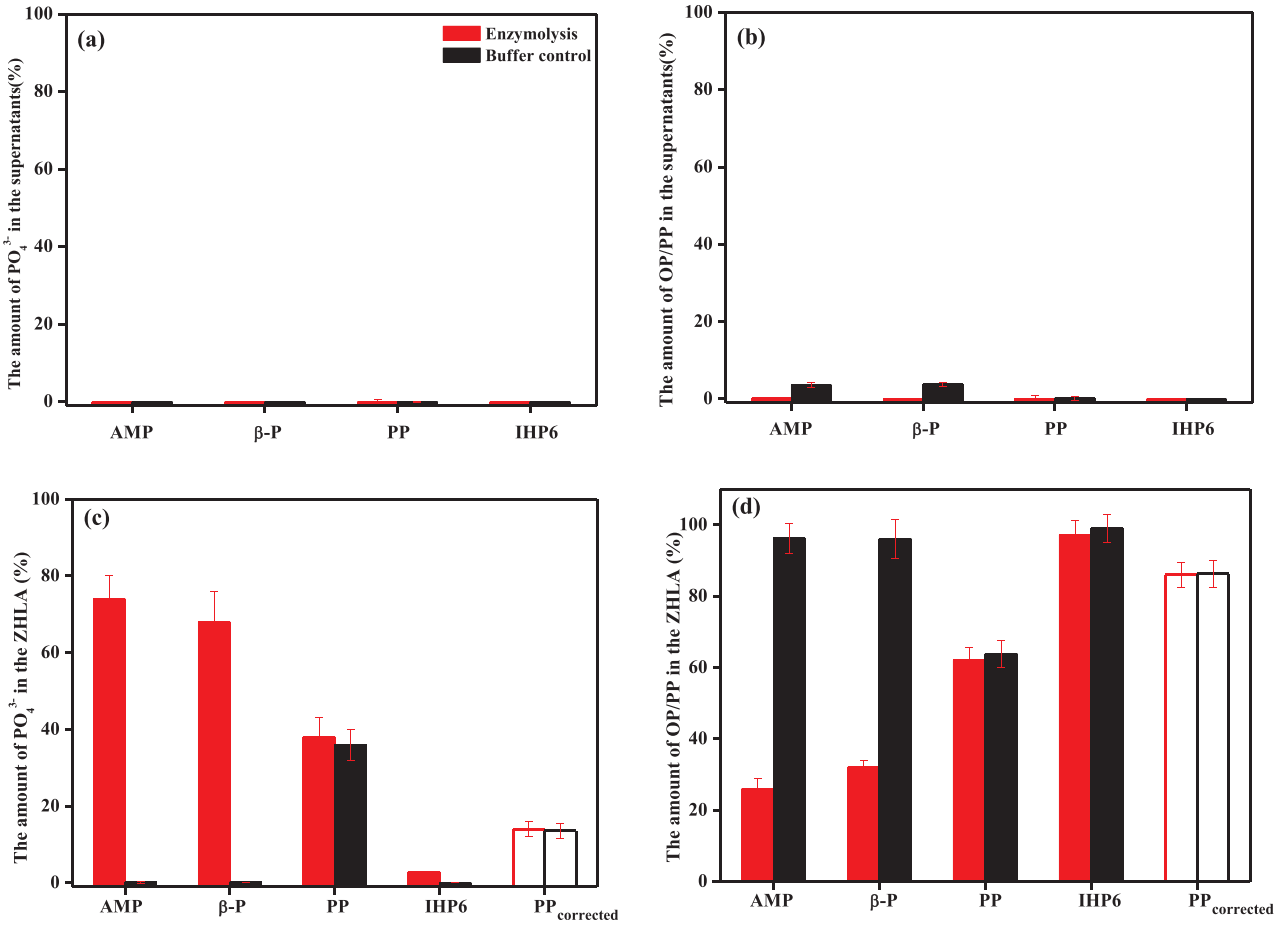

Fig. 7. Stabilization of model P compounds by ZHLA: (a) degradation of OP or PP in the supernatants; (b) desorption of OP and PP in the supernatants; (c) degradation of OP or PP in the residues; (d) unhydrolyzed OP/PP in the residues. The corrected bars of PP in (c) and (d) represented the authentic content of degradation and unhydrolyzed PP in residues, respectively, after eliminating hydrolysis effects of HCl extraction on PP.

ZHLA can therefore be a compelling candidate as a functional material for P control.

4. Conclusion

The effects of synthetic zeolite loaded with HA and La on the immobilization of OP and PP under enzymolysis and photolysis are investigated. The primary conclusions of this study are summarized as follows. This synthetic material exhibits excellent performance to capture P with its porous structure, small particle size, and large specific surface areas. It is found that successfully loaded $La(OH)_3$ binds with the HA in the synthetic zeolite mainly by the chelation of carboxylic acid and phenolic hydroxyl groups in the HA. Moreover, PO_4^{3-} could not be released from AMP, β-P, PP, and IHP6 in natural lake water by solar lights. Although practically all AMP and β-P, and 25% IHP6 could be photodegraded into PO_4^{3-} by Fenton's reagents, HA and $La(OH)_3$ could protect the OP from hydrolyzing into PO_4^{3-} mainly because of the shading effect of HA and the formation of stable OP–La chelates. In addition, OP and PP could be easily hydrolyzed into PO_4^{3-} by phosphatase; however, this enzymatic hydrolysis efficiency substantially drops with the presence of La and HA. The activity of AP is reduced by $La(OH)_3$ nanorods, which mainly cause the hydrolysis rate of AMP and

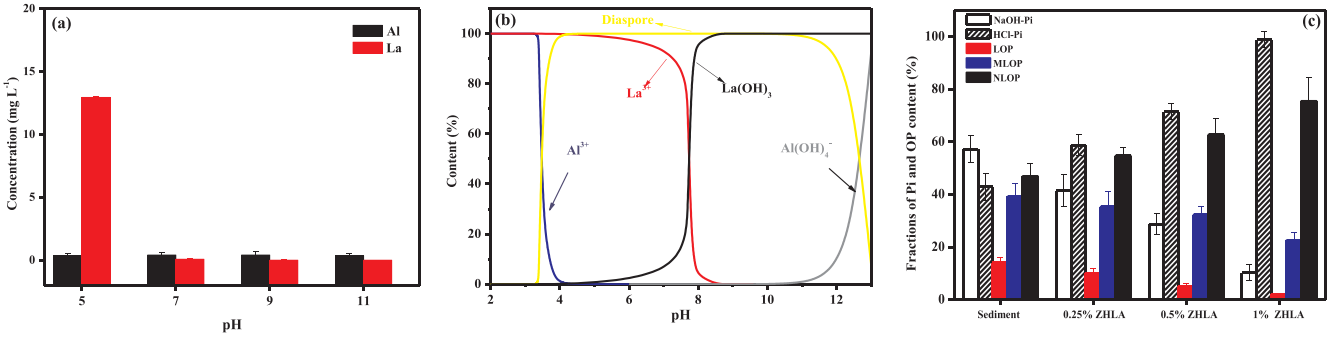

Fig. 8. (a): The concentrations of released Al^{3+} and La^{3+} from pH 5.0 to 9.0; (b) the thermodynamic states of La^{3+} and Al^{3+} at pH 2–13 and 25 °C simulated by visual MINTEQ; (c): The content of various Pi and OP fractions in raw sediment and sediment amended with different doses of ZHLA. NaOH-Pi and HCl-Pi: Pi extratted with NaOH and HCl, respectively, in the SMT. LOP: Labile OP; MLOP: Moderately labile OP; NLOP: Non-labile OP, in the Ivanoff method.

β-P to drop. The formation of stable HA–La–PP/IHP6 or La–PP/IHP6 chelates also prevents the hydrolysis of PP and IHP6. It is further observed that ZHLA exhibits an excellent performance in the immobilization of PO_4^{3-}, OP, and PP as a capping material in the sediment incubation experiments. The ZHLA has a high potential as a type of commercial sediment capping material for P control.

Declaration of Competing Interest

The authors declare that they have no known competing financial interests or personal relationships that could have appeared to influence the work reported in this paper.

Acknowledgements

This study was supported by the Strategic Priority Research Program of the Chinese Academy of Sciences (Grant No.: XDA23050203) and the National Natural Science Foundation of China (Grant No. 41373100). Additional support was provided by the Key Research and Development Program of Shandong Province (Grant No. 2019GSF109002).

Appendix A. Supplementary data

Supplementary data to this article can be found online at https://doi.org/10.1016/j.cej.2019.123791.

References

[1] Z. Wang, M. Xing, W. Fang, D. Wu, One-step synthesis of magnetite core/zirconia shell nanocomposite for high efficiency removal of phosphate from water, Appl. Surf. Sci. 366 (2016) 67–77.
[2] E.K. Read, M. Ivancic, P. Hanson, B.J. Cade-Menun, K.D. McMahon, Phosphorus speciation in a eutrophic lake by 31P NMR spectroscopy, Water Res. 62 (2014) 229–240.
[3] D.W. Schindler, S.R. Carpenter, S.C. Chapra, R.E. Hecky, D.M. Orihel, Reducing phosphorus to curb lake eutrophication is a success, Environ. Sci. Technol. 50 (2016) 8923–8929.
[4] C. Li, H. Yu, S. Tabassum, L. Li, D. Wu, Z. Zhang, H. Kong, P. Xu, Effect of calcium silicate hydrates (CSH) on phosphorus immobilization and speciation in shallow lake sediment, Chem. Eng. J. 317 (2017) 844–853.
[5] Y. Fan, Y. Li, D. Wu, C. Li, H. Kong, Application of zeolite/hydrous zirconia composite as a novel sediment capping material to immobilize phosphorus, Water Res. 123 (2017) 1–11.
[6] M. Zamparas, I. Zacharias, Restoration of eutrophic freshwater by managing internal nutrient loads. A review, Sci. Total Environ. 496 (2014) 551–562.
[7] J. Xie, Z. Wang, D. Wu, Z. Zhang, H. Kong, Synthesis of zeolite/aluminum oxide hydrate from coal fly ash: a new type of adsorbent for simultaneous removal of cationic and anionic pollutants, Ind. Eng. Chem. Res. 52 (2013) 14890–14897.
[8] J. Xie, Z. Wang, D. Wu, H. Kong, Synthesis and properties of zeolite/hydrated iron oxide composite from coal fly ash as efficient adsorbent to simultaneously retain cationic and anionic pollutants from water, Fuel 116 (2014) 71–76.
[9] J. Goscianska, M. Ptaszkowska-Koniarz, M. Frankowski, M. Franus, R. Panek, W. Franus, Removal of phosphate from water by lanthanum-modified zeolites obtained from fly ash, J. Colloid Interface Sci. 513 (2018) 72–81.
[10] R. Xu, M. Zhang, R.J.G. Mortimer, G. Pan, Enhanced phosphorus locking by novel lanthanum/aluminum-hydroxide composite: implications for eutrophication control, Environ. Sci. Technol. 51 (2017) 3418–3425.
[11] E. Diatloff, C.J. Asher, F.W. Smith, Use of GEOCHEM-PC to predict rare earth element (REE) species in nutrient solutions, Plant Soil 155 (1993) 251–254.
[12] Y. Zhu, F. Wu, W. Feng, S. Liu, J.P. Giesy, Interaction of alkaline phosphatase with minerals and sediments: activities, kinetics and hydrolysis of organic phosphorus, Colloids Surf., A 495 (2016) 46–53.
[13] S. Ding, X. Bai, C. Fan, L. Zhang, Caution needed in pretreatment of sediments for refining phosphorus-31 nuclear magnetic resonance analysis: results from a comprehensive assessment of pretreatment with ethylenediaminetetraacetic acid, J. Environ. Qual. 39 (2010) 1668–1678.
[14] R. Huang, B. Wan, M. Hultz, J.M. Diaz, Y. Tang, Phosphatase-mediated hydrolysis of linear polyphosphates, Environ. Sci. Technol. 52 (2018) 1183–1190.
[15] Y. Zhu, W. Feng, S. Liu, Z. He, X. Zhao, Y. Liu, J. Guo, J.P. Giesy, F. Wu, Bioavailability and preservation of organic phosphorus in lake sediments: insights from enzymatic hydrolysis and(31)P nuclear magnetic resonance, Chemosphere 211 (2018) 50–61.
[16] X. Li, Y. Zhou, G. Liu, H. Lei, D. Zhu, Mechanisms of the photochemical release of phosphate from resuspended sediments under solar irradiation, Sci. Total Environ. 595 (2017) 779–786.
[17] Y. Zhu, F. Wu, Z. He, J. Guo, X. Qu, F. Xie, J.P. Giesy, H. Liao, F. Guo, Characterization of organic phosphorus in lake sediments by sequential fractionation and enzymatic hydrolysis, Environ. Sci. Technol. 47 (2013) 7679–7687.
[18] D. Özkundakci, D.P. Hamilton, M.M. Gibbs, Hypolimnetic phosphorus and nitrogen dynamics in a small, eutrophic lake with a seasonally anoxic hypolimnion, Hydrobiologia 661 (2011) 5–20.
[19] P. Boguta, V. D'Orazio, N. Senesi, Z. Sokołowska, K. Szewczuk-Karpisz, Insight into the interaction mechanism of iron ions with soil humic acids. The effect of the pH and chemical properties of humic acids, J. Environ. Manage. 245 (2019) 367–374.
[20] Y. Lei, M. Saakes, R.D. van der Weijden, C.J.N. Buisman, Effects of current density, bicarbonate and humic acid on electrochemical induced calcium phosphate precipitation, Chem. Eng. J. 342 (2018) 350–356.
[21] J. Pertusatti, A.G.S. Prado, Buffer capacity of humic acid: thermodynamic approach, J. Colloid Interface Sci. 314 (2007) 484–489.
[22] Y. Zhu, F. Wu, Z. He, J.P. Giesy, W. Feng, Y. Mu, C. Feng, X. Zhao, H. Liao, Z. Tang, Influence of natural organic matter on the bioavailability and preservation of organic phosphorus in lake sediments, Chem. Geol. 397 (2015) 51–60.
[23] S. Hong, M. Elimelech, Chemical and physical aspects of natural organic matter (NOM) fouling of nanofiltration membranes, J. Membr. Sci. 132 (1997) 159–181.
[24] G. Zhao, Y. Sheng, J. Wang, Z. Li, J. Yang, Optimized digestion methods: organic phosphorus sequential extraction, total phosphorus, and nitrogen simultaneous determination in sediments, J. Soils Sediments 18 (2018) 2072–2080.
[25] H. Xie, Q. Zheng, S. Wang, C. Ma, G. Gao, N. Bing, Z. Sun, Capture of phosphates in surface water by TiO_2 nanoparticles under UV irradiation, Particuology 14 (2014) 98–102.
[26] C. Zhao, L.E. Arroyo-Mora, A.P. DeCaprio, V.K. Sharma, D.D. Dionysiou, K.E. O'Shea, Reductive and oxidative degradation of iopamidol, iodinated X-ray contrast media, by Fe(III)-oxalate under UV and visible light treatment, Water Res. 67 (2014) 144–153.
[27] J. Zhu, B. Qu, M. Li, Phosphorus mobilization in the Yeyahu Wetland: phosphatase enzyme activities and organic phosphorus fractions in the rhizosphere soils, Int. Biodeterior. Biodegrad. 124 (2017) 304–313.
[28] P. Chanaud, A. Julbe, P. Vaija, M. Persin, L. Cot, Study of lanthanum-based colloidal sols formation, J. Mater. Sci. 29 (1994) 4244–4251.
[29] K.I. Aspila, H. Agemian, A.S.Y. Chau, Semiautomated method for determination of inorganic, organic and total phosphate in sediments, Analyst 101 (1976) 187–197.
[30] G.B. Douglas, D.P. Hamilton, M.S. Robb, G. Pan, B.M. Spears, M. Lurling, Guiding principles for the development and application of solid-phase phosphorus adsorbents for freshwater ecosystems, Aquat. Ecol. 50 (2016) 385–405.
[31] K. Reitzel, H.S. Jensen, S. Egemose, pH dependent dissolution of sediment aluminum in six Danish lakes treated with aluminum, Water Res. 47 (2013) 1409–1420.
[32] S. Wang, Y. Peng, Natural zeolites as effective adsorbents in water and wastewater treatment, Chem. Eng. J. 156 (2010) 11–24.
[33] H. Tanaka, Y. Sakai, R. Hino, Formation of Na-A and -X zeolites from waste solutions in conversion of coal fly ash to zeolites, Mater. Res. Bull. 37 (2002) 1873–1884.
[34] M. Mazloumi, N. Shahcheraghi, A. Kajbafvala, S. Zanganeh, A. Lak, M.S. Mohajerani, S.K. Sadrnezhaad, 3D bundles of self-assembled lanthanum hydroxide nanorods via a rapid microwave-assisted route, J. Alloys Compd. 473 (2009) 283–287.
[35] W.A. Khanday, S.A. Majid, S. Chandra Shekar, R. Tomar, Synthesis and characterization of various zeolites and study of dynamic adsorption of dimethyl methyl phosphate over them, Mater. Res. Bull. 48 (2013) 4679–4686.
[36] R.H. Hesas, M.S. Baei, H. Rostami, J. Gardy, A. Hassanpour, An investigation on the capability of magnetically separable Fe_3O_4/mordenite zeolite for refinery oily wastewater purification, J. Environ. Manage. 241 (2019) 525–534.
[37] W. Xue, D. Huang, G. Zeng, J. Wan, C. Zhang, R. Xu, M. Cheng, R. Deng, Nanoscale zero-valent iron coated with rhamnolipid as an effective stabilizer for immobilization of Cd and Pb in river sediments, J. Hazard. Mater. 341 (2018) 381–389.
[38] R. Andreozzi, M. Raffaele, P. Nicklas, Pharmaceuticals in STP effluents and their solar photodegradation in aquatic environment, Chemosphere 50 (2003) 1319–1330.
[39] J. Ma, N.J.D. Graham, Degradation of atrazine by manganese-catalysed ozonation: influence of humic substances, Water Res. 33 (1999) 785–793.
[40] J. Vansteveninck, Influence of metal ions on hydrolysis of polyphosphates, Biochemistry 5 (1966) 1998-+.
[41] P.W.A. Hubner, R.M. Milburn, Hydrolysis of pyrophosphate to ortho-phosphate promoted by cobalt(iii) – evidence for the role of polynuclear species, Inorg. Chem. 19 (1980) 1267–1272.
[42] B.L. Turner, A.W. Cheesman, H.Y. Godage, A.M. Riley, B.V.L. Potter, Determination of neo- and D-chiro-inositol hexakisphosphate in soils by solution P-31 NMR spectroscopy, Environ. Sci. Technol. 46 (2012) 4994–5002.
[43] M. Férid, K. Horchani-Naifer, Synthesis, crystal structure and vibrational spectra of a new form of diphosphate NaLaP2O7, Mater. Res. Bull. 39 (2004) 2209–2217.
[44] W. Hami, A. Zegzouti, M. Daoud, D. Zambon, M. Rossi, A. Vergara, F. Capitelli, A. Altomare, R. Rizzi, Synthesis, structural characterization and luminescent properties of Tb3+-doped $AgLaP_2O_7$ phosphors, Ceram. Int. 44 (2018) 19184–19190.
[45] Z. Liu, S. Shang, K.-L. Chiu, S. Jiang, F. Dai, Fabrication of conductive and flame-retardant bifunctional cotton fabric by polymerizing pyrrole and doping phytic acid, Polym. Degrad. Stab. 167 (2019) 277–282.
[46] S. Erdogan, A. Baysal, O. Akba, C. Hamamci, Interaction of metals with humic acid isolated from oxidized coal, Pol. J. Environ. Stud. 16 (2007) 671–675.
[47] Y. Wang, S. Liu, Y. Cai, S. Deng, B. Han, R. Han, Q. Li, Y. Wang, La(OH)3:Ln3+ (Ln = Sm, Er, Gd, Dy, and Eu) nanorods synthesized by a facile hydrothermal

method and their enhanced photocatalytic degradation of Congo red in the aqueous solution, Ceram. Int. 40 (2014) 5091–5095.
[48] C. Lesueur, M. Pfeffer, M. Fuerhacker, Photodegradation of phosphonates in water, Chemosphere 59 (2005) 685–691.
[49] V. Ruban, J.F. Lopez-Sanchez, P. Pardo, G. Rauret, H. Muntau, P. Quevauviller, Harmonized protocol and certified reference material for the determination of extractable contents of phosphorus in freshwater sediments – a synthesis of recent works, Fresenius J. Anal. Chem. 370 (2001) 224–228.
[50] D.B. Ivanoff, K.R. Reddy, S. Robinson, Chemical fractionation of organic phosphorus in selected histosols, Soil Sci. 163 (1998) 36–45.